CO_2 Conversion to Butene via a Tandem Photovoltaic-Electrochemical/Photothermocatalytic Process: A Co-Design Approach to Coupled Microenvironments

Kyra M. K. Yap[1-3‡], Aisulu Aitbekova[3,4‡], Matthew Salazar[3,5‡], Tobias A. Kistler[3,6], Melanie Rodríguez Pabón[2,3], Magel P. Su[3,4], Nicholas B. Watkins[3,5], Sang-Won Lee[1-3], Peter Agbo[3,6], Adam Z. Weber[3,6], Jonas C. Peters[3,5*], Theodor Agapie[3,5*], Adam C. Nielander[1,3*], Harry A. Atwater[3,4*], Thomas F. Jaramillo[1-3*], Alexis T. Bell[3,6,7*]

[1]SUNCAT Center for Interface Science and Catalysis, SLAC National Accelerator Laboratory, Menlo Park, CA 94025, USA

[2]Department of Chemical Engineering, Stanford University, Stanford, CA 94305, USA

[3]Liquid Sunlight Alliance, California Institute of Technology, Pasadena, CA 91125, USA

[4]Department of Applied Physics and Materials Science, California Institute of Technology, Pasadena, CA 91125, USA

[5]Division of Chemistry and Chemical Engineering, California Institute of Technology, Pasadena, CA 91125, USA

[6]Lawrence Berkeley National Laboratory, Berkeley, CA 94720, USA

[7]Department of Chemical and Biomolecular Engineering, University of California, Berkeley, Berkeley, CA 94720, USA

‡ Equal contributions

[*]Corresponding authors

Jonas C. Peters: jpeters@caltech.edu

Theodor Agapie: agapie@caltech.edu

Adam C. Nielander: anieland@slac.stanford.edu

Harry A. Atwater: haa@caltech.edu

Thomas F. Jaramillo: jaramillo@stanford.edu

Alexis T. Bell: alexbell@berkeley.edu

Abstract

We developed a tandem, unassisted, solar-driven electrochemical and photothermocatalytic process for the single-pass conversion of CO_2 to butene using only simulated solar irradiation as the energetic input. The two-step process involves electrochemical CO_2 reduction (CO_2R) to ethylene followed by ethylene dimerization to butene. We assessed two unassisted electrochemical setups to concentrate ethylene in the CO_2R reactor, achieving concentrations up to 5.4 vol.% with 1.8% average solar-to-ethylene conversion and 5.6% average CO_2-to-ethylene single-pass conversion under 1-sun illumination. When passed through the photothermocatalytic ethylene oligomerization reactor, we generated 600 ppm of butene under 3-sun illumination. Through analysis of this process, we identified that the presence of H_2, CO, and H_2O leads to rapid deactivation of the Ni-based ethylene oligomerization catalyst.

Introduction

The conversion of carbon dioxide (CO_2) to building block chemicals using renewable energy offers an attractive means for decarbonizing the chemical industry. Butene is a key platform chemical that is currently produced as a byproduct of petroleum refining[1,2] and is used to produce plastics, lubricating oils, and antioxidants.[3] Current electrochemical solar-driven CO_2 reduction (CO_2R) is primarily limited to C_1-C_2 products, namely carbon monoxide (19 % solar-to-fuel efficiency) and ethylene (3-5 % solar-to-fuel efficiency).[4–7] Electrochemical conversion of CO_2 to products with more than three carbon atoms, for example butene, remains difficult and has not been demonstrated in a single-step.[8] Potential approaches to upgrading CO_2 to longer-chain hydrocarbons include cascade tandem processes, which couple CO_2R to downstream thermocatalytic processes.[9–12] In this work, we coupled a solar-driven CO_2R reactor, producing ethylene, to a heterogeneous photothermocatalytic ethylene oligomerization reactor for butene generation. Both reactors are powered solely by solar irradiation, resulting in a process that leverages the entire solar spectrum to convert waste CO_2 into butene. The strategy and implementation described herein illustrate an attractive conceptual approach to decarbonizing the production of a broad range of multi-carbon industrial fuels and chemicals.

A key challenge for the successful operation of a tandem solar-driven electrochemical-photothermocatalytic system is the co-design of the two processes such that both work at the same pressure and the effluent from the electrochemical system is compatible with the catalyst used in the photothermocatalytic system.[9,13] Specifically, solar-driven CO_2R is carried out at ambient temperature and pressure[4,14], whereas thermocatalytic ethylene oligomerization normally occurs at elevated temperatures (80-140 °C) and pressures (30-150 atm).[15–17] Combining these processes requires operating the CO_2R reactor to maximize the concentration of ethylene and minimize the concentrations of other gaseous products, which may inhibit the oligomerization process. Driving CO_2R using only sunlight imposes a maximum power operating constraint (per unit area) on the CO_2R reactor.[18–20] Under unassisted conditions, this limits the per unit area CO_2 conversion for an integrated solar-driven CO_2R reactor and has consequences for the concentration of ethylene in

the outlet gas stream delivered to the photothermocatalytic reactor. Similar barriers exist for the photothermocatalytic reactor, which must be engineered to maximize the conversion of solar irradiation to thermal energy. Moreover, the catalyst used for ethylene oligomerization must be capable of utilizing gas inlet streams containing C_2H_4, CO, CO_2, CH_4, H_2O, and H_2 that are produced from the CO_2R reactor.[21,22] The catalyst constraint is notable because ethylene oligomerization is usually performed with pure ethylene using a nickel-based catalyst[23,24], and only a handful of studies have reported the impact of other compounds (e.g., CO_2, CO, and H_2)[25,26].

Herein, we present an unassisted, solar-driven tandem system that couples electrochemical CO_2 reduction with photothermocatalytic, heterogeneously catalyzed ethylene oligomerization to produce butene in a single pass. We examined two designs for the CO_2R reactor. The first, referred to as a PV-EC reactor, integrates the photovoltaic (PV) component into an electrochemical (EC) reactor containing a cathode comprised of a gas diffusion electrode (GDE). The second, a PV-MEA reactor, comprises a separated PV component and membrane electrode assembly (MEA). The PV-MEA reactor produced an ethylene concentration of ~5.4 vol.% as compared to only ~0.6 vol.% for the PV-EC reactor. To perform the photothermocatalytic step, we modified a photothermocatalytic reactor integrated with a selective solar absorber layer[27], and carried out ethylene oligomerization using a supported nickel catalyst. We demonstrated that this catalyst generated butene using a dilute stream of ethylene in the presence of up to ~18 vol.% CO and ~5 vol.% H_2. However, we observed a loss of catalyst activity with time, which we attribute to the presence of CO and H_2O in the gas stream fed to the photothermocatalytic reactor.

Results and Discussion

The solar-driven electrochemical and thermal reactors were co-designed for butene generation. For the electrochemical system, we targeted an outlet ethylene concentration of >5% and aimed to maximize the ratio of ethylene to other gaseous products (e.g., CO). Additionally, to facilitate simpler process design and improve potential energy efficiency via heat integration, we strove to integrate the PV and EC components.[28–32] For the photothermocatalytic reactor, the system had to reach temperatures high enough to achieve ethylene oligomerization at atmospheric pressure. The oligomerization catalyst also had to be capable of performing the desired chemistry in the presence of gaseous byproduct impurities (e.g., CO, H_2, H_2O). These criteria formed the basis for the design of the tandem process illustrated in **Figure 1**.

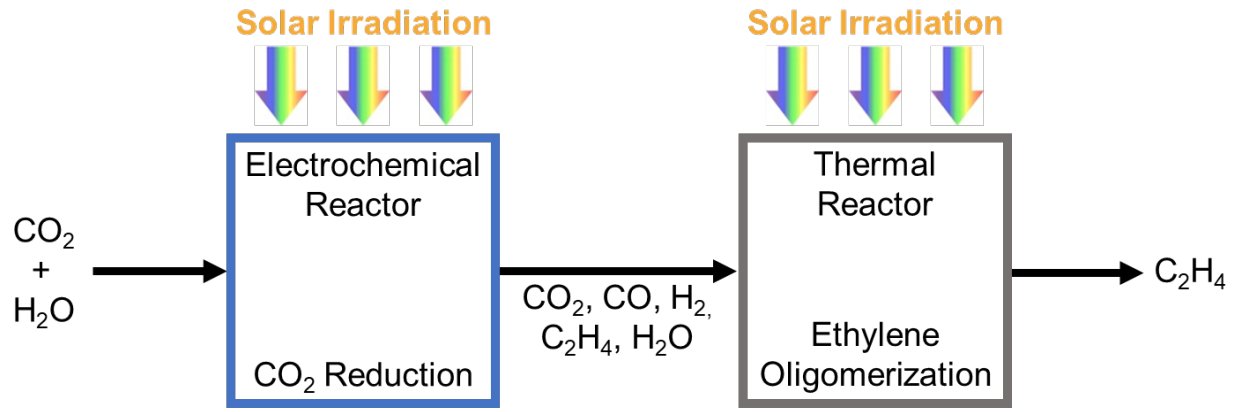

Figure 1. Schematic of the solar-driven tandem process involving the coupling of a CO_2 reduction reactor for CO_2 to ethylene conversion with a thermocatalytic reactor to convert ethylene to butene via ethylene oligomerization.

Design and performance of the solar-driven CO_2 reduction system

Two CO_2R reactor configurations were examined to investigate the tradeoff between integration and separation of the PV and EC functionalities within a single reactor. In an integrated PV-EC solar reactor, the PV component imposes an upper limit on the maximum power that can be achieved in the reactor, a key consideration for achieving a concentrated ethylene outlet gas stream.[18–20]

The first design involved an integrated PV-EC system as shown in **Figure 2A**. This reactor consists of an integrated photoanode combining a serially connected Si solar cell to a Ni anode catalyst (**see supplemental methods**). The anode to cathode area ratio is 4:1 to reduce the overpotential required at the planar photoanode to match the current density (and current as $A_{cathode}$ = 1 cm^2) of the cathode (J_{geo}). The cathode catalyst comprises a thin layer of Cu sputtered onto carbon paper, which serves as a gas diffusion layer. To enhance the formation of ethylene relative to other products, the surface of the Cu film is modified with an electrodeposited film derived from diphenyliodonium (DPI) (**Figure S1**). This film is hydrophobic, decreasing H_2 evolution by lowering the availability of water at the catalyst surface and reducing the diffusion coefficient of CO, enabling further conversion of CO to C_{2+} products.[33–35]

The electrochemical performance of the Cu-DPI modified cathode was determined separately from operation under illumination. The results in **Figure S2** show the current-voltage characteristic of the PV and EC components. The products formed on the Cu-DPI cathode during CO_2R were measured for cathode current densities of J_{geo} = -60 mA cm^{-2}, -120 mA cm^{-2}, -180 mA cm^{-2}, to identify the operating condition that would maximize ethylene concentration in the outlet gas stream (**Figure S3, Table S1**). In the presence of the DPI-derived film, the maximum ethylene Faradaic efficiency (FE) was ~41% at J_{geo} = -120 mA cm^{-2}. When coupled to the PV component, the intersection of the current-voltage curves for the PV, designed to be integrated into the photoanode, and the EC reactor occurred near 60 mA (J_{geo} = -60 mA cm^{-2}), which was the

maximum current density predicted to be attainable for prolonged unassisted operation of the system (**Figure S2**). **Figure S4** shows that the unassisted PV-EC device operated at an initial cathodic current density of approximately -65 mA cm^{-2} with an illumination at 100 mW cm^{-2} and a CO_2 inlet flow rate of 5 sccm. A peak ethylene concentration of ~0.6 vol.% in the effluent gas stream was achieved after 20 min (**Figure S4**). These results correspond to an average solar-to-ethylene efficiency of 1.3% and an average CO_2-to-ethylene single-pass conversion of 0.87% (**Note S1**). However, over time the concentration of ethylene in the outlet gas stream decreased and was accompanied by an increase in the H_2 concentration. These trends are attributed to the loss of the electrodeposited DPI film throughout the reaction which was confirmed by SEM and XPS (**Figure S1**). Loss of the polymer film also led to a decrease in the current density, which is attributed to a change in the operating point, as the temperature of the PV increased and the cathode performance degraded due to the loss of the DPI film. As shown in **Figure S5**, the PV and EC polarization curves shifted over the course of reaction such that the operating point decreased to lower current densities.[36–41]

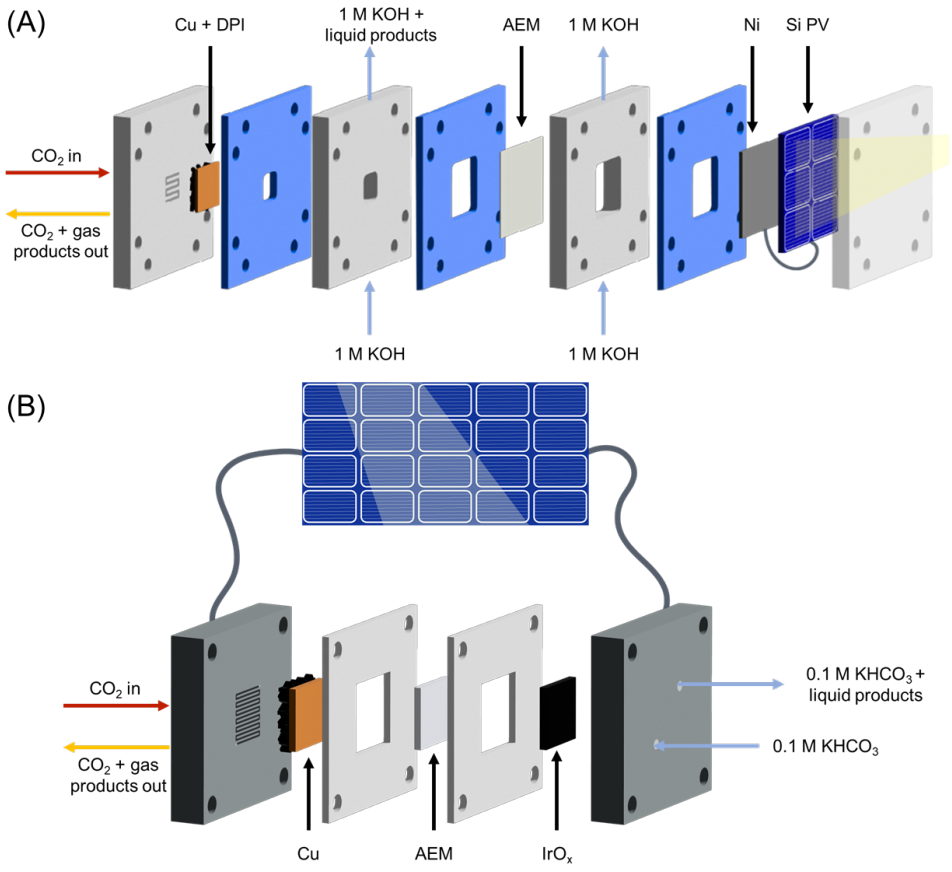

Figure 2. Schematics of the two solar-driven electrochemical CO_2R reactors. (A) PV-EC CO_2R reactor. The reactor utilizes a 1 cm^2 porous sputtered Cu-DPI/PTFE treated carbon paper cathode, and an integrated photoanode consisting of a 4 cm^2 Ni foil integrated to a 16 cm^2, 0.2 W Si solar cell. CO_2 is fed through the serpentine channel at 5 sccm while 1 M KOH is fed at 2 mL min^{-1} through the anolyte and catholyte chambers which are separated by a Sustainion anion exchange

membrane (AEM). The anode and cathode are wired together to complete the circuit. (B) PV-MEA CO_2R reactor. The reactor utilizes a 5 cm^2 porous sputtered Cu/PTFE treated carbon paper cathode and a 5 cm^2 IrO_x/carbon paper anode. The anode and cathode are separated by a Sustainion AEM. CO_2 is fed into the serpentine channel at the back of the cathode at 10 sccm, while 0.1 M $KHCO_3$ is fed through the back of the anode at 2 mL min^{-1}. Three 1.2-W, 50-cm^2 Si solar cells are connected in series to the MEA. The PV component of both reactors is illuminated with an intensity of 100 mW cm^{-2}.

Since the peak ethylene concentration in the effluent stream of the PV-EC reactor was much lower than the target value of 5 vol.%, we considered a second, less integrated, solar-driven design (**Figure 2B**). This design involved a separate PV array directly connected to a 5 cm^2 MEA. Removal of the geometric constraint present in the PV-EC reactor allowed the PV-MEA reactor to operate at J_{geo} = -120 mA cm^{-2}. The PV-EC reactor utilized the Cu-DPI cathode, the PV-MEA reactor was operated with only the sputtered Cu film deposited on carbon paper, since inclusion of the DPI-derived polymer film in the case of the PV-MEA system led to degradation of the film and loss of ethylene selectivity (**Figure S6**). The performance of the MEA reactor operated under electrochemical conditions at J_{geo} = -120 mA cm^{-2} (I = 600 mA) is shown in **Figures 3A** and **B**. Under these conditions, the MEA achieved an ethylene FE of 36% and a CO FE of 14%.

The PV array for the PV-MEA was designed so that the intersection of the power and load curves occurred well within the light-limited regime of the PV component, as shown in **Figure 3C**. The unassisted operation of the PV-MEA resulted in a total current of approximately 610 mA (**Figure S7**) and a cathodic current density of approximately -122 mA cm^{-2} under illumination with 100 mW cm^{-2}. The inlet CO_2 flow rate was set to 10 sccm, and the outlet flow rate was measured to be ~5 sccm; an expected result as it is well-established that the lower effluent flow rate can be attributed to conversion of CO_2 to C_{2+} products and to CO_2 crossover from the cathode to the anode compartments of the MEA.[42,43] Under illumination conditions, the concentration of ethylene in the outlet gas stream was ~5.4 vol.% and was fairly constant for the duration of the 4 h reaction (**Figure 3D**). This corresponds to an average solar-to-ethylene efficiency of 1.8% and an average CO_2-to-ethylene single-pass conversion of 5.6%. While the ethylene concentration measured for the PV-MEA reactor was an order of magnitude higher than that measured for the PV-EC, the CO concentration was also higher, 18 vol.% for the PV-MEA reactor versus 1.4 vol.% for the PV-EC reactor. However, since the targeted ethylene concentration of >5 vol.% was achieved using the PV-MEA reactor, we focused on this reactor for the evaluation of the tandem system.

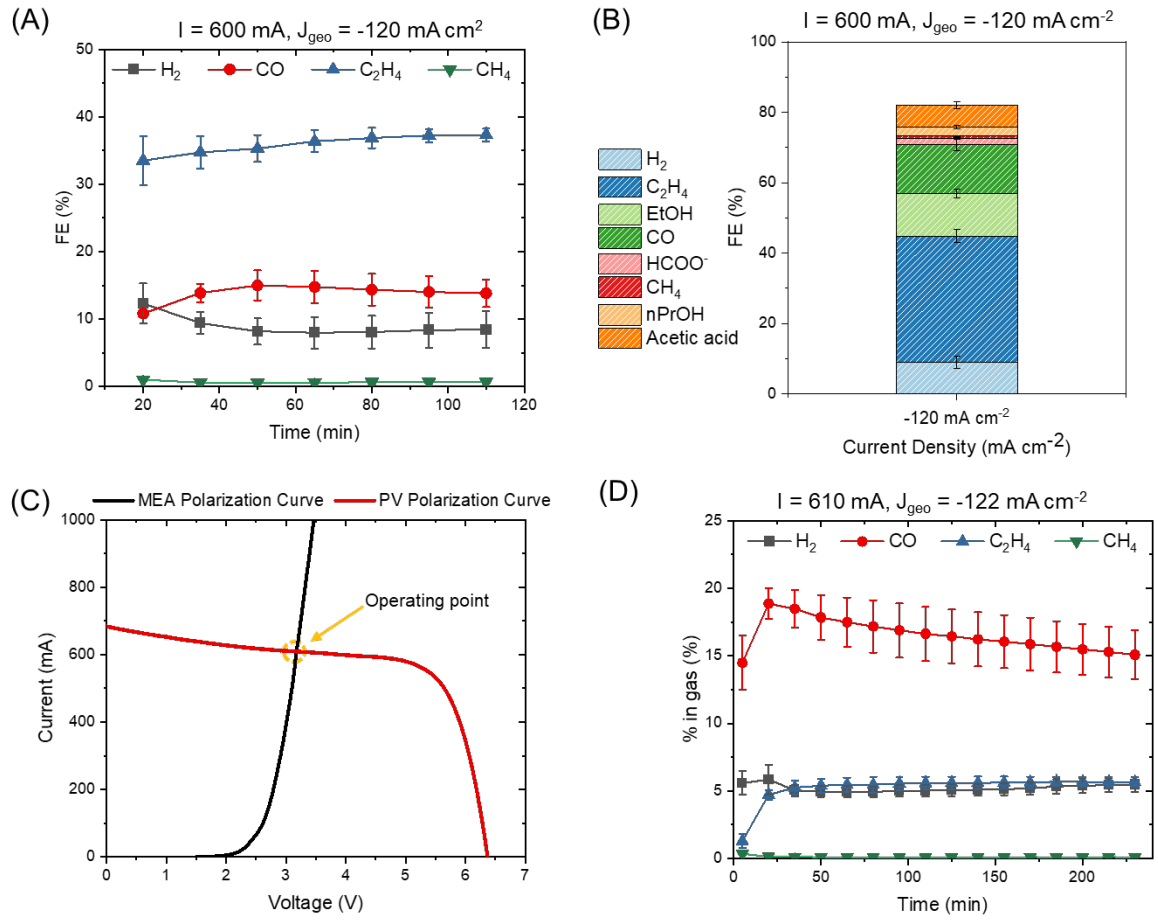

Figure 3. Overview of performance for the PV-MEA CO_2 reduction reactor. (A) Gaseous product FE vs. time for the MEA reactor under dark galvanostatic conditions of I = 600 mA (J_{geo} = -120 mA cm^{-2}). (B) Average FE for the MEA reactor under reaction conditions described in (A), including liquid CO_2R products collected from the anolyte reservoir at the end of the experiment. The missing FE is attributed to product re-oxidation at the anode and liquid product trapping in the serpentine channel of the cathode.[44] (C) Polarization curves for the MEA reactor with a sputtered Cu catalyst and three serially connected 1.2 W Si photovoltaics. (D) Composition of the outlet gas from the unassisted operation of the PV-MEA device under illumination of 100 mW cm^{-2}. **Figure S8** gives the corresponding FE for the unassisted PV-MEA. Error bars represent experiments repeated at least in triplicate.

Design of the photothermocatalytic reactor

The photothermocatalytic reactor converts sunlight into thermal energy to reach the temperatures required for ethylene oligomerization. The design and operation of the photothermocatalytic reactor is described by Su et al.[27] Briefly, from top to bottom (**Figure 4A**) the photothermocatalytic reactor consists of a quartz window to allow illumination, a vacuum chamber to minimize heat

losses to the environment, and a selective solar absorber to convert light into thermal energy. A plug flow reactor containing the supported nickel catalyst is placed into a hole in the lower flange of the photothermocatalytic reactor. To further minimize heat losses to the environment, the reactor is placed in an insulated box.

The key requirement for the ethylene oligomerization catalyst is that it operates with a dilute ethylene stream containing a substantial concentration of CO. While homogeneous transition-metal catalysts (e.g., Ti, Ni, Zr) are utilized for industrial ethylene oligomerization, they require harmful organic solvents, expensive catalyst recovery costs, and de-coking.[45,46] By contrast, heterogeneous Ni catalysts are appealing since they remove the need for catalyst separation.[46] For this study, we used Ni supported on either commercial alumina-silica (SIRAL-30) or aluminated SBA-15.[23,46–48] The catalysts were prepared using previously reported procedures.[23]

Performance of the tandem PV-MEA/photothermocatalytic system

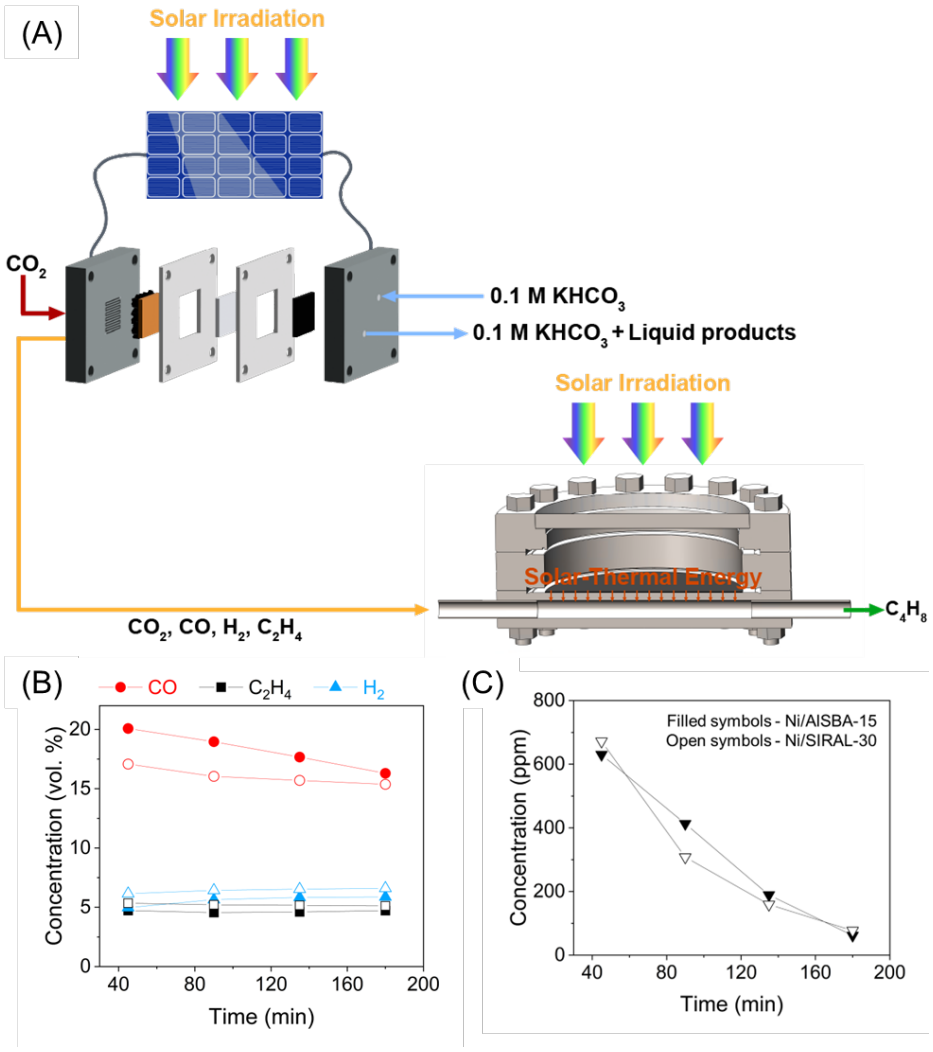

Figure 4. (A) Schematic for the tandem solar-driven electrochemical CO_2 reduction and photothermocatalytic oligomerization process. CO_2 gas is fed into a 5 cm^2 PV-MEA at 10 sccm,

illuminated at 100 mW cm^{-2}, with the outlet gas fed directly to the photothermocatalytic reactor. The photothermocatalytic reactor consists of a selective photoabsorber to convert solar irradiation into thermal energy and operates at 150 ˚C under illumination of 300 mW cm^{-2}. Concentrations of (B) H_2, C_2H_4, CO, and (C) butene in the outlet of the photothermocatalytic reactor. Filled symbols stand for a supported nickel (2 wt. %) on SBA-15, Ni/AlSBA-15 and open symbols stand for 4 wt. % Ni on SIRAL-30, Ni/SIRAL-30.

Figure 4A shows the connection between the PV-MEA and photothermocatalytic reactors. The performance of this solar-driven tandem system is shown in **Figures 4B** and **4C.** The effluent stream from the tandem setup had an initial CO concentration of 18 – 20 vol.% that decreased with time, whereas the initial ethylene concentration was ~5.4 vol.% and remained constant with time. Both oligomerization catalysts (Ni/SIRAL and Ni/SBA-15) initially produced ~600 ppm of butene (0.01% CO_2 to butene conversion), but this concentration steadily decreased over time. Both oligomerization catalysts exhibited similar deactivation profiles. Formation of butene as the single oligomerization product is attributed to the low ethylene partial pressure.

To assess whether the Ni-SIRAL-30 catalyst utilized in the tandem system is intrinsically stable for ethylene dimerization and to identify possible causes for the deactivation observed in **Figure 4C**, we conducted reactions in a stainless steel gas-flow reactor, heated to 150 °C (the operating temperature of the photothermocatalytic reactor under 300 mW cm^{-2}) using resistive heating with input streams mimicking the outlet of the PV-MEA. **Figure 5** demonstrates stable formation of butenes with a dilute ethylene stream (5 vol.% ethylene in CO_2), resulting in a butene concentration of 1000 ppm, corresponding to a 4% butene yield. Introducing 5 vol.% H_2 to the reactor feed gradually decreased butene formation and generated ethane, attributed to ethylene hydrogenation (**Figure S9**). Saturating the stream with H_2O vapor or introducing 20 vol. % CO led to catalyst deactivation. These results show that while H_2 leads to the formation of ethane, H_2O and CO lead to rapid catalyst deactivation. We suspect that H_2O poisons the catalyst because it adsorbs on the cationic Ni sites responsible for ethylene oligomerization.[49] The results shown in **Figure 5A,B** indicate that sustained dimerization of ethylene to butene necessitates minimizing the concentrations of H_2 and CO in the effluent from the CO_2R reactor and removal of the remaining H_2 and CO, and all H_2O from the PV-MEA effluent stream, via condensation, adsorption or H_2 pumping.[50,51] To further reduce any separations requirements, the concentrations of H_2 and CO produced in the PV-MEA reactor could potentially be minimized via a range of approaches, including by pulsed electrolysis (carefully controlled by light pulsing), or by using different ionomer coatings to improve the ethylene:CO and ethylene:H_2 selectivity on the Cu catalyst**.**[52–55] While these approaches may reduce the Faradaic selectivity to CO and H_2, CO will likely always be present in the effluent stream in non-negligible concentrations. In the conversion of CO_2 to ethylene, CO is a key intermediate and byproduct, and is generated in a 6:1 molar ratio of CO to ethylene (by Faraday's law). Hence, developing technologies for the selective separation of CO from the PV-MEA effluent gas stream is a worthwhile strategy for improving the future performance of the tandem PV-MEA photothermocatalytic process.

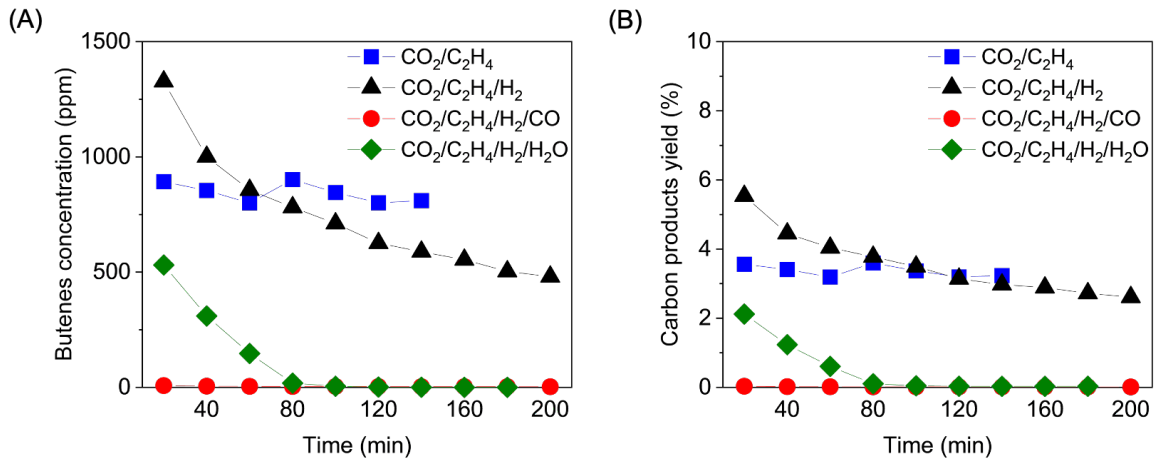

Figure 5. Performance of Ni/SIRAL-30 at 150 °C. Concentrations of butenes (A) and carbon products yield (B) under various conditions mimicking gas concentrations produced in the PV-MEA device: CO_2/C_2H_4 corresponds to 5 vol.% C_2H_4, balance CO_2; $CO_2/C_2H_4/H_2$ is 5 vol.% C_2H_4, 5 vol.% H_2, balance CO_2; $CO_2/C_2H_4/H_2/CO$ is 5 vol.% C_2H_4, 5 vol.% H_2, 20 vol.% CO, balance CO_2; and $CO_2/C_2H_4/H_2/H_2O$ is 5 vol.% C_2H_4, 5 vol.% H_2, balance CO_2, saturated with water. The total flow rate for all compositions was 5 sccm.

Conclusions

We co-designed coupled microenvironments to develop a tandem, unassisted, solar-driven electrochemical and photothermocatalytic process for the single-pass conversion of CO_2 to the C_4 product, butene. This involved electrochemical CO_2R-to-ethylene followed by ethylene oligomerization to butene. To achieve this goal, we assessed two unassisted electrochemical setups. In the first setup, we employed a monolithically integrated PV-EC flow cell designed for use with a photoanode, operated at a current of 60 mA. We observed a maximum ethylene FE of 41%, which corresponded to a concentration of ~0.6 vol.% ethylene in the outlet gas stream, a solar-to-ethylene conversion of ~1.3% and a single-pass CO_2 conversion of ~0.87%. Recognizing that the low effluent concentration of ethylene from this system would hinder dimerization in the photothermocatalytic reactor, we evaluated a second CO_2R reactor, a PV-MEA cell in which the PV element is physically separated from the MEA-type reactor. This unit operated at a current of 610 mA and produced an outlet ethylene concentration of ~5.4 vol.%, corresponding to an average solar-to-ethylene conversion of ~1.8% and average CO_2-to-ethylene single pass conversion of ~5.6%. The outlet gas stream from the PV-MEA system was fed to the photothermocatalytic reactor containing Ni-based catalysts (Ni-AlSBA-15 or Ni-SIRAL-30). When the photothermocatalytic reactor was heated to 150 °C by 3-sun illumination and operated at ambient pressure, the initial concentration of butene was 600 ppm in the outlet gas stream. However, rapid deactivation of both Ni-based catalysts occurred with time on stream. Additional experiments revealed that for the concentrations of ethylene and CO_2 and the flow rate of effluent from the PV-MEA reactor, Ni-SIRAL-30 produced a stable butene concentration of 1000 ppm. This work

revealed that the deactivation observed for the tandem system is attributable to the presence of H_2, which hydrogenates ethylene to ethane, and to the presence of CO and H_2O, both of which cause catalyst deactivation, an area for future improvement. Overall, we demonstrated unassisted, solar driven conversion of CO_2 and water vapor to butene in a tandem PV-MEA and photothermocatalytic system. Our work provides a critical demonstration of the co-design of solar technologies to develop a solar-driven tandem process that converts CO_2 into butene.

Author Contributions

K.M.K.Y., A.A., and M.S. contributed equally to the ideation of the project, completion of experiments, and writing of the manuscript. M.R.P., S.L., N.B.W. and T.A.K. contributed to the completion of electrochemical experimental results and characterization. M.P. contributed to the thermal experimental results. T.A.K., P.A., A.Z.N., J.C.P., T.A., A.C.N., H.A.A., T.F.J., and A.T.B. aided in the development of the project.

Conflicts of Interest

The authors declare no conflicts of interest.

Acknowledgements

This work was funded by the Liquid Sunlight Alliance, which is supported by the U.S. Department of Energy, Office of Science, Office of Basic Energy Sciences, Fuels from Sunlight Hub under Award Number DE-SC0021266. Part of this work was performed in the nano@Stanford labs, which are supported by the National Science Foundation as part of the National Nanotechnology Coordinated Infrastructure under award ECCS-1542152. Some of this work was also performed at the Stanford Nano Shared Facilities (SNSF), supported by the National Science Foundation under award ECCS-2026822. K.M.K.Y. acknowledges the Chevron Energy Fellowship and the Stanford DARE fellowship for partial support. A.A. acknowledges the Kavli Nanoscience Institute Postdoctoral Fellowship.

References

(1) Barnett, B. R.; Parker, S. T.; Paley, M. V.; Gonzalez, M. I.; Biggins, N.; Oktawiec, J.; Long, J. R. Thermodynamic Separation of 1-Butene from 2-Butene in Metal–Organic Frameworks with Open Metal Sites. *J. Am. Chem. Soc.* **2019**, *141* (45), 18325–18333. https://doi.org/10.1021/jacs.9b09942.

(2) Metzger, E. D.; Brozek, C. K.; Comito, R. J.; Dincă, M. Selective Dimerization of Ethylene to 1-Butene with a Porous Catalyst. *ACS Cent. Sci.* **2016**, *2* (3), 148–153. https://doi.org/10.1021/acscentsci.6b00012.

(3) *1-Butene Market: Global Industry Trend Analysis 2012 to 2017 and Forecast 2017 - 2025*. Persistence Market Research. https://www.persistencemarketresearch.com/market-research/1-butene-market.asp (accessed 2024-04-09).

(4) Cheng, W.-H.; Richter, M. H.; Sullivan, I.; Larson, D. M.; Xiang, C.; Brunschwig, B. S.; Atwater, H. A. CO_2 Reduction to CO with 19% Efficiency in a Solar-Driven Gas Diffusion Electrode Flow Cell under Outdoor Solar Illumination. *ACS Energy Lett.* **2020**, *5* (2), 470–476. https://doi.org/10.1021/acsenergylett.9b02576.

(5) Gao, J.; Li, J.; Liu, Y.; Xia, M.; Finfrock, Y. Z.; Zakeeruddin, S. M.; Ren, D.; Grätzel, M. Solar Reduction of Carbon Dioxide on Copper-Tin Electrocatalysts with Energy Conversion Efficiency near 20%. *Nat. Commun.* **2022**, *13* (1), 5898. https://doi.org/10.1038/s41467-022-33049-7.

(6) Zhou, X.; Xiang, C. Comparative Analysis of Solar-to-Fuel Conversion Efficiency: A Direct, One-Step Electrochemical CO_2 Reduction Reactor versus a Two-Step, Cascade Electrochemical CO_2 Reduction Reactor. *ACS Energy Lett.* **2018**, *3* (8), 1892–1897. https://doi.org/10.1021/acsenergylett.8b01077.

(7) Gurudayal; Bullock, J.; Srankó, D. F.; Towle, C. M.; Lum, Y.; Hettick, M.; Scott, M. C.; Javey, A.; Ager, J. Efficient Solar-Driven Electrochemical CO_2 Reduction to Hydrocarbons and Oxygenates. *Energy Environ. Sci.* **2017**, *10* (10), 2222–2230. https://doi.org/10.1039/C7EE01764B.

(8) Zhou, Y.; Martín, A. J.; Dattila, F.; Xi, S.; López, N.; Pérez-Ramírez, J.; Yeo, B. S. Long-Chain Hydrocarbons by CO_2 Electroreduction Using Polarized Nickel Catalysts. *Nat. Catal.* **2022**, *5* (6), 545–554. https://doi.org/10.1038/s41929-022-00803-5.

(9) Garg, S.; Xie, Z.; Chen, J. G. Tandem Reactors and Reactions for CO_2 Conversion. *Nat. Chem. Eng.* **2024**, *1* (2), 139–148. https://doi.org/10.1038/s44286-023-00020-2.

(10) Zhang, J.; Kang, X.; Yan, Y.; Ding, X.; He, L.; Li, Y. Cascade Electrocatalytic and Thermocatalytic Reduction of CO_2 to Propionaldehyde. *Angew. Chem. Int. Ed.* **2024**, *63* (12), e202315777. https://doi.org/10.1002/anie.202315777.

(11) Biswas, A. N.; Xie, Z.; Xia, R.; Overa, S.; Jiao, F.; Chen, J. G. Tandem Electrocatalytic–Thermocatalytic Reaction Scheme for CO_2 Conversion to C3 Oxygenates. *ACS Energy Lett.* **2022**, *7* (9), 2904–2910. https://doi.org/10.1021/acsenergylett.2c01454.

(12) Biswas, A. N.; Winter, L. R.; Xie, Z.; Chen, J. G. Utilizing CO_2 as a Reactant for C3 Oxygenate Production via Tandem Reactions. *JACS Au* **2023**, *3* (2), 293–305. https://doi.org/10.1021/jacsau.2c00533.
(13) Lee, M. G.; Li, X.-Y.; Ozden, A.; Wicks, J.; Ou, P.; Li, Y.; Dorakhan, R.; Lee, J.; Park, H. K.; Yang, J. W.; Chen, B.; Abed, J.; dos Reis, R.; Lee, G.; Huang, J. E.; Peng, T.; Chin, Y.-H. (Cathy); Sinton, D.; Sargent, E. H. Selective Synthesis of Butane from Carbon Monoxide Using Cascade Electrolysis and Thermocatalysis at Ambient Conditions. *Nat. Catal.* **2023**, *6* (4), 310–318. https://doi.org/10.1038/s41929-023-00937-0.
(14) Singh, M. R.; Clark, E. L.; Bell, A. T. Effects of Electrolyte, Catalyst, and Membrane Composition and Operating Conditions on the Performance of Solar-Driven Electrochemical Reduction of Carbon Dioxide. *Phys. Chem. Chem. Phys.* **2015**, *17* (29), 18924–18936. https://doi.org/10.1039/C5CP03283K.
(15) Finiels, A.; Fajula, F.; Hulea, V. Nickel-Based Solid Catalysts for Ethylene Oligomerization – a Review. *Catal. Sci. Technol.* **2014**, *4* (8), 2412–2426. https://doi.org/10.1039/C4CY00305E.
(16) Andrei, R. D.; Popa, M. I.; Fajula, F.; Hulea, V. Heterogeneous Oligomerization of Ethylene over Highly Active and Stable Ni-AlSBA-15 Mesoporous Catalysts. *J. Catal.* **2015**, *323*, 76–84. https://doi.org/10.1016/j.jcat.2014.12.027.
(17) Lallemand, M.; Finiels, A.; Fajula, F.; Hulea, V. Ethylene Oligomerization over Ni-Containing Mesostructured Catalysts with MCM-41, MCM-48 and SBA-15 Topologies. In *Studies in Surface Science and Catalysis*; Xu, R., Gao, Z., Chen, J., Yan, W., Eds.; From Zeolites to Porous MOF Materials - The 40th Anniversary of International Zeolite Conference; Elsevier, 2007; Vol. 170, pp 1863–1869. https://doi.org/10.1016/S0167-2991(07)81071-8.
(18) Yap, K. M. K.; Wei, W. J.; Pabón, M. R.; King, A. J.; Bui, J. C.; Wei, L.; Lee, S.-W.; Weber, A. Z.; Bell, A. T.; Nielander, A. C.; Jaramillo, T. F. Modeling Diurnal and Annual Ethylene Generation from Solar-Driven Electrochemical CO_2 Reduction Devices. *Energy Environ. Sci.* **2024**. https://doi.org/10.1039/D4EE00545G.
(19) Yap, K. M. K.; Lee, S.-W.; Steiner, M. A.; Avilés Acosta, J. E.; Kang, D.; Kim, D.; Warren, E. L.; Nielander, A. C.; Jaramillo, T. F. A Framework for Understanding Efficient Diurnal CO_2 Reduction Using Si and GaAs Photocathodes. *Chem Catal.* **2023**, *3* (6), 100641. https://doi.org/10.1016/j.checat.2023.100641.
(20) King, A. J.; Bui, J. C.; Bell, A. T.; Weber, A. Z. Establishing the Role of Operating Potential and Mass Transfer in Multicarbon Product Generation for Photoelectrochemical CO_2 Reduction Cells Using a Cu Catalyst. *ACS Energy Lett.* **2022**, *7* (8), 2694–2700. https://doi.org/10.1021/acsenergylett.2c01041.
(21) Albdour, S. A.; Haddad, Z.; Sharaf, O. Z.; Alazzam, A.; Abu-Nada, E. Micro/Nano-Encapsulated Phase-Change Materials (ePCMs) for Solar Photothermal Absorption and Storage: Fundamentals, Recent Advances, and Future Directions. *Prog. Energy Combust. Sci.* **2022**, *93*, 101037. https://doi.org/10.1016/j.pecs.2022.101037.

(22) Li, S.; Haussener, S. Design and Operational Guidelines of Solar-Driven Catalytic Conversion of CO_2 and H_2 to Fuels. *Appl. Energy* **2023**, *334*, 120617. https://doi.org/10.1016/j.apenergy.2022.120617.
(23) Lee, M.; Yoon, J. W.; Kim, Y.; Yoon, J. S.; Chae, H.-J.; Han, Y.-H.; Hwang, D. W. Ni/SIRAL-30 as a Heterogeneous Catalyst for Ethylene Oligomerization. *Appl. Catal. Gen.* **2018**, *562*, 87–93. https://doi.org/10.1016/j.apcata.2018.06.004.
(24) Tuskaev, V. A.; Zubkevich, S. V.; Saracheno, D.; Gagieva, S. Ch.; Dorovatovskii, P. V.; Kononova, E. G.; Khrustalev, V. N.; Zarubin, D. N.; Bulychev, B. M.; Kissin, Y. V. Nickel(II) Complexes with Tripodal NNN Ligands as Homogenous and Supported Catalysts for Ethylene Oligomerization. *Mol. Catal.* **2019**, *464*, 29–38. https://doi.org/10.1016/j.mcat.2018.12.018.
(25) Andrei, R. D.; Borodina, E.; Minoux, D.; Nesterenko, N.; Dath, J.-P.; Cammarano, C.; Hulea, V. Ethylene Oligomerization from Diluted Stream over Ni-Containing Heterogeneous Catalysts. *Ind. Eng. Chem. Res.* **2020**, *59* (5), 1746–1752. https://doi.org/10.1021/acs.iecr.9b05576.
(26) Kimura, K.; A-i, H.; Ozaki, A. Tracer Study of Ethylene Dimerization over Nickel Oxide-Silica Catalyst. *J. Catal.* **1970**, *18* (3), 271–280. https://doi.org/10.1016/0021-9517(70)90322-2.
(27) Su, M.; Aitbekova, A.; Salazar, M.; Li, X.; Xiong, S.; Espinosa, M.; Peters, J. C.; Agapie, T.; Atwater, H. A. A Photothermocatalytic Reactor and Selective Solar Absorber for Sustainable Fuel Synthesis by Ethylene Oligomerization. **In Preparation**.
(28) Modestino, M. A.; Haussener, S. An Integrated Device View on Photo-Electrochemical Solar-Hydrogen Generation. *Annu. Rev. Chem. Biomol. Eng.* **2015**, *6* (Volume 6, 2015), 13–34. https://doi.org/10.1146/annurev-chembioeng-061114-123357.
(29) Tembhurne, S.; Haussener, S. Controlling Strategies to Maximize Reliability of Integrated Photo-Electrochemical Devices Exposed to Realistic Disturbances. *Sustain. Energy Fuels* **2019**, *3* (5), 1297–1306. https://doi.org/10.1039/C8SE00441B.
(30) Xiang, C.; Weber, A. Z.; Ardo, S.; Berger, A.; Chen, Y.; Coridan, R.; Fountaine, K. T.; Haussener, S.; Hu, S.; Liu, R.; Lewis, N. S.; Modestino, M. A.; Shaner, M. M.; Singh, M. R.; Stevens, J. C.; Sun, K.; Walczak, K. Modeling, Simulation, and Implementation of Solar-Driven Water-Splitting Devices. *Angew. Chem. Int. Ed.* **2016**, *55* (42), 12974–12988. https://doi.org/10.1002/anie.201510463.
(31) Tembhurne, S.; Nandjou, F.; Haussener, S. A Thermally Synergistic Photo-Electrochemical Hydrogen Generator Operating under Concentrated Solar Irradiation. *Nat. Energy* **2019**, *4* (5), 399–407. https://doi.org/10.1038/s41560-019-0373-7.
(32) Kistler, T. A.; Um, M. Y.; Cooper, J. K.; Sharp, I. D.; Agbo, P. Exploiting Heat Transfer to Achieve Efficient Photoelectrochemical CO_2 Reduction under Light Concentration. *Energy Environ. Sci.* **2022**, *15* (5), 2061–2070. https://doi.org/10.1039/D1EE03957A.
(33) Watkins, N. B.; Wu, Y.; Nie, W.; Peters, J. C.; Agapie, T. In Situ Deposited Polyaromatic Layer Generates Robust Copper Catalyst for Selective Electrochemical CO_2 Reduction at

Variable pH. *ACS Energy Lett.* **2023**, *8* (1), 189–195. https://doi.org/10.1021/acsenergylett.2c02002.
(34) Thevenon, A.; Rosas-Hernández, A.; Peters, J. C.; Agapie, T. In-Situ Nanostructuring and Stabilization of Polycrystalline Copper by an Organic Salt Additive Promotes Electrocatalytic CO_2 Reduction to Ethylene. *Angew. Chem.* **2019**, *131* (47), 17108–17114. https://doi.org/10.1002/ange.201907935.
(35) Watkins, N. B.; Schiffer, Z. J.; Lai, Y.; Musgrave, C. B. I.; Atwater, H. A.; Goddard, W. A. I.; Agapie, T.; Peters, J. C.; Gregoire, J. M. Hydrodynamics Change Tafel Slopes in Electrochemical CO_2 Reduction on Copper. *ACS Energy Lett.* **2023**, *8* (5), 2185–2192. https://doi.org/10.1021/acsenergylett.3c00442.
(36) Popović, S.; Smiljanić, M.; Jovanovič, P.; Vavra, J.; Buonsanti, R.; Hodnik, N. Stability and Degradation Mechanisms of Copper-Based Catalysts for Electrochemical CO_2 Reduction. *Angew. Chem.* **2020**, *132* (35), 14844–14854. https://doi.org/10.1002/ange.202000617.
(37) Jännsch, Y.; Leung, J. J.; Hämmerle, M.; Magori, E.; Wiesner-Fleischer, K.; Simon, E.; Fleischer, M.; Moos, R. Pulsed Potential Electrochemical CO_2 Reduction for Enhanced Stability and Catalyst Reactivation of Copper Electrodes. *Electrochem. Commun.* **2020**, *121*, 106861. https://doi.org/10.1016/j.elecom.2020.106861.
(38) Rendón-Calle, A.; Low, Q. H.; Hong, S. H. L.; Builes, S.; Yeo, B. S.; Calle-Vallejo, F. How Symmetry Factors Cause Potential- and Facet-Dependent Pathway Shifts during CO_2 Reduction to CH_4 on Cu Electrodes. *Appl. Catal. B Environ.* **2021**, *285*, 119776. https://doi.org/10.1016/j.apcatb.2020.119776.
(39) van Dyk, E. E.; Scott, B. J.; Meyer, E. L.; Leitch, A. W. R. Temperature Dependence of Performance of Crystalline Silicon Photovoltaic Modules. *South Afr. J. Sci.* **2000**.
(40) Wysocki, J. J.; Rappaport, P. Effect of Temperature on Photovoltaic Solar Energy Conversion. *J. Appl. Phys.* **1960**, *31* (3), 571–578. https://doi.org/10.1063/1.1735630.
(41) Kistler, T. A.; Agbo, P. Current Loss Analysis in Photoelectrochemical Devices. *APL Mater.* **2020**, *8* (3), 031107. https://doi.org/10.1063/1.5142561.
(42) Larrazábal, G. O.; Strøm-Hansen, P.; Heli, J. P.; Zeiter, K.; Therkildsen, K. T.; Chorkendorff, I.; Seger, B. Analysis of Mass Flows and Membrane Cross-over in CO_2 Reduction at High Current Densities in an MEA-Type Electrolyzer. *ACS Appl. Mater. Interfaces* **2019**, *11* (44), 41281–41288. https://doi.org/10.1021/acsami.9b13081.
(43) Garg, S.; Xu, Q.; B. Moss, A.; Mirolo, M.; Deng, W.; Chorkendorff, I.; Drnec, J.; Seger, B. How Alkali Cations Affect Salt Precipitation and CO_2 Electrolysis Performance in Membrane Electrode Assembly Electrolyzers. *Energy Environ. Sci.* **2023**, *16* (4), 1631–1643. https://doi.org/10.1039/D2EE03725D.
(44) Jin Sa, Y.; Woo Lee, C.; Young Lee, S.; Na, J.; Lee, U.; Jeong Hwang, Y. Catalyst–Electrolyte Interface Chemistry for Electrochemical CO_2 Reduction. *Chem. Soc. Rev.* **2020**, *49* (18), 6632–6665. https://doi.org/10.1039/D0CS00030B.

(45) Moussa, S.; Concepción, P.; Arribas, M. A.; Martínez, A. Nature of Active Nickel Sites and Initiation Mechanism for Ethylene Oligomerization on Heterogeneous Ni-Beta Catalysts. *ACS Catal.* **2018**, *8* (5), 3903–3912. https://doi.org/10.1021/acscatal.7b03970.
(46) Seufitelli, G. V. S.; Gustafson, R. Novel Ni-SIRAL Catalyst for Heterogeneous Ethylene Oligomerization. *Ind. Eng. Chem. Res.* **2022**, *61* (12), 4286–4299. https://doi.org/10.1021/acs.iecr.2c00052.
(47) Kwon, M.-H.; Yoon, J. S.; Lee, M.; Hwang, D. W.; Kim, Y.; Park, M. B.; Chae, H.-J. One-Pot Cascade Ethylene Oligomerization Using Ni/Siral-30 and H-ZSM-5 Catalysts. *Appl. Catal. Gen.* **2019**, *572*, 226–231. https://doi.org/10.1016/j.apcata.2018.12.005.
(48) Luan, Z.; Hartmann, M.; Zhao, D.; Zhou, W.; Kevan, L. Alumination and Ion Exchange of Mesoporous SBA-15 Molecular Sieves. *Chem. Mater.* **1999**, *11* (6), 1621–1627. https://doi.org/10.1021/cm9900756.
(49) Forget, S.; Olivier-Bourbigou, H.; Delcroix, D. Homogeneous and Heterogeneous Nickel-Catalyzed Olefin Oligomerization: Experimental Investigation for a Common Mechanistic Proposition and Catalyst Optimization. *ChemCatChem* **2017**, *9* (12), 2408–2417. https://doi.org/10.1002/cctc.201700348.
(50) Kistler, T. A.; Prabhakar, R. R.; Agbo, P. A Recirculation System for Concentrating CO_2 Electrolyzer Products. *Sustain. Energy Fuels* **2024**, *8* (10), 2292–2298. https://doi.org/10.1039/D3SE01506H.
(51) Sarswat, A.; Sholl, D. S.; Lively, R. P. Achieving Order of Magnitude Increases in CO_2 Reduction Reaction Efficiency by Product Separations and Recycling. *Sustain. Energy Fuels* **2022**, *6* (20), 4598–4604. https://doi.org/10.1039/D2SE01156E.
(52) Kim, C.; Weng, L.-C.; Bell, A. T. Impact of Pulsed Electrochemical Reduction of CO_2 on the Formation of C2+ Products over Cu. *ACS Catal.* **2020**, *10* (21), 12403–12413. https://doi.org/10.1021/acscatal.0c02915.
(53) Casebolt, R.; Levine, K.; Suntivich, J.; Hanrath, T. Pulse Check: Potential Opportunities in Pulsed Electrochemical CO_2 Reduction. *Joule* **2021**, *5* (8), 1987–2026. https://doi.org/10.1016/j.joule.2021.05.014.
(54) Kim, C.; Bui, J. C.; Luo, X.; Cooper, J. K.; Kusoglu, A.; Weber, A. Z.; Bell, A. T. Tailored Catalyst Microenvironments for CO_2 Electroreduction to Multicarbon Products on Copper Using Bilayer Ionomer Coatings. *Nat. Energy* **2021**, *6* (11), 1026–1034. https://doi.org/10.1038/s41560-021-00920-8.
(55) Idros, M. N.; Wu, Y.; Duignan, T.; Li, M.; Cartmill, H.; Maglaya, I.; Burdyny, T.; Wang, G.; Rufford, T. E. Effect of Dispersing Solvents for an Ionomer on the Performance of Copper Catalyst Layers for CO_2 Electrolysis to Multicarbon Products. *ACS Appl. Mater. Interfaces* **2023**, *15* (45), 52461–52472. https://doi.org/10.1021/acsami.3c11096.